JACS
JOURNAL OF THE AMERICAN CHEMICAL SOCIETY
Article
pubs.acs.org/JACS

Ideal Polyethylene Nanocrystals

Anna Osichow,[†] Christian Rabe,[‡] Karsten Vogtt,[‡] Theyencheri Narayanan,[§] Ludger Harnau,[∥,⊥] Markus Drechsler,[#] Matthias Ballauff,*[,‡,¶] and Stefan Mecking*[,†]

[†]Chair of Chemical Materials Science, Department of Chemistry, University of Konstanz, Universitätsstr. 10, D-78457 Konstanz, Germany

[‡]Helmholtz-Zentrum Berlin for Materials and Energy, Hahn Meitner-Platz 1, D-14109 Berlin, Germany

[§]European Synchrotron Radiation Facility, F-38043 Grenoble, France

[∥]Max Planck Institute for Intelligent Systems, D-70569 Stuttgart, Germany

[⊥]Institute for Theoretical Physics IV, University of Stuttgart, D-70550 Stuttgart, Germany

[#]Bayreuth Institute of Macromolecular Research (BIMF), University of Bayreuth, D-95440 Bayreuth, Germany

[¶]Department of Physics, Humboldt University Berlin, Newtonstr. 15, D-12489 Berlin, Germany

Supporting Information

ABSTRACT: The water-soluble catalyst precursor [[(2,4,6-(3,5-$(CF_3)_2C_6H_3)_3$-C_6H_2)-N=C(H)-(3-(9-anthryl)-2-O-C_6H_3)-κ^2-N,O]Ni(CH_3)(TPPTS)] (TPPTS = tri-(sodiumphenylsulfonate)phosphine) polymerizes ethylene to aqueous dispersions of highly ordered nanoscale crystals (crystallinity χ(DSC) $\geq$ 90%) of strictly linear polyethylene (<0.7 methyl-branches/1000 carbon atoms, $M_n = 4.2 \times 10^5$ g mol^{-1}). SAXS in combination with cryo-TEM confirms this unusually high degree of order (χ(SAXS) = 82%) and shows the nanoparticles to possess a very thin amorphous layer on the crystalline lamella, just sufficient to accommodate a loop, but likely no entanglements. This ideal chain-folded structure is corroborated by annealing studies on the aqueous-dispersed nanoparticles, which show that the chain can move through the crystal as evidenced by lamella thickening without disturbing the crystalline order as concluded from an unaltered low thickness of the amorphous layers. These ideal chain-folded polyethylene nanocrystals arise from the crystallization in the confined environment of a nanoparticle and a deposition of the growing polymer chain on the crystal growth front as the chain is formed by the catalyst.

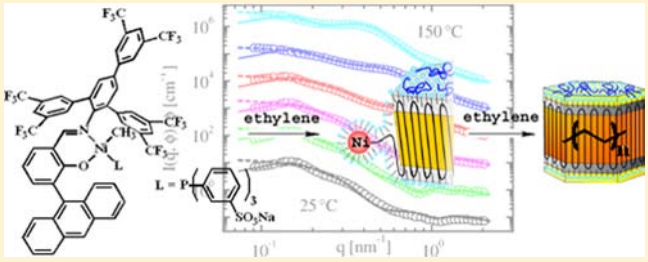

INTRODUCTION

Crystalline order is ubiquitous in condensed phases. Practically, it is decisive for the mechanical properties of many materials. In high molecular weight polymeric materials the degree of crystalline order is limited. Even for linear polymers devoid of any branches that disturb crystallization, a substantial portion of the material is present as an amorphous phase containing loops and entanglements. This results from intertwined chains not being able to unravel during crystal formation. Such entanglements improve the mechanical properties and hinder the processing strongly. To overcome this problem, it is desirable to access nonentangled 'nascent' polymers from the polymerization process.[1] A possible approach is a compartmentalization during polymerization, and furthermore a 'perfect' ordered deposition of the forming chain on a nanocrystal growth front.

Such a compartmentalization scenario can be put into practice by catalytic ethylene polymerization in aqueous systems to polyethylene nanoparticle dispersions.[2] The crystallization of the polymer occurs in a limited volume containing very little material (a few polymer chains at the most) as provided by the individual nanoparticles. The dispersed nanocrystals formed consist of a single crystalline lamella covered by thin amorphous polymer layers which contain all defects such as branches and entanglements.[3] Annealing of such crystals below the melting temperature leads to a thickening of the crystalline lamella that can be studied with high precision.[4] This thickening of the crystalline lamella can be understood in terms of an unlooping of polymer chains within a single nanoparticle. However, the role of short chain branches and entanglements remained unclear in all studies done so far, and consequently the realization of this concept to 'perfect' polymer nanocrystals had remained elusive.

We now report how unusually high degrees of order can be obtained by crystallization during ethylene polymerization in the compartmented space of nanoparticles in aqueous systems. A key to these findings is a new water-soluble catalyst, which produces high molecular weight polyethylene particles virtually devoid of any branches. The degree of crystallinity and thus the

Received: May 24, 2013
Published: July 15, 2013

   dx.doi.org/10.1021/ja4052334 | J. Am. Chem. Soc. 2013, 135, 11645−11650

high degree of order of these dispersed nanoparticles are revealed by SAXS in combination with cryo-TEM.[5] Based on careful annealing studies of the particles we argue that the PE-nanocrystals thus generated represent ideal polymer crystals.

RESULTS AND DISCUSSION

In the catalytic polymerization in aqueous emulsion employed,[2b] an aqueous surfactant solution of a water-soluble catalyst precursor is exposed to ethylene. Upon activation for polymerization the catalyst becomes lipophilic, and polyethylene chain growth will result in immediate formation of a surfactant-stabilized particle in which further polymerization occurs, to yield nanoscale single-crystals (Figure 1).[3]

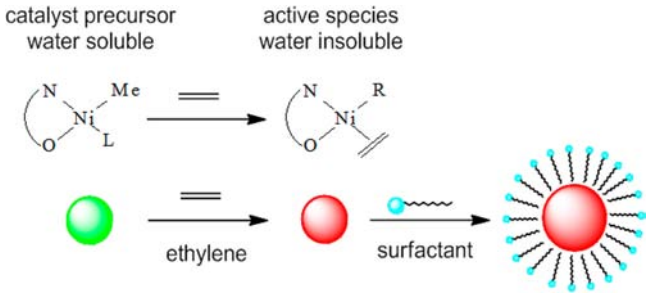

Figure 1. Particle formation by catalytic polymerization in an aqueous system.

From ongoing screening of a large number of new catalysts, the novel complex **1** was found to be exceptional in that it reproducibly affords highly ordered ideal polyethylene nanocrystals (for synthesis and characterization of the precatalyst cf. Supporting Information, SI). This catalyst produces highly linear polyethylene (M_n = 4.2 × 10^5 g mol^{-1} and M_w/M_n = 1.4; see SI) virtually devoid of any branches within experimental error of the ^{13}C NMR microstructure analysis (<0.7 methyl-branches/1000 carbon atoms, Figure S2). An unusually high crystallinity of $\chi \geq 90\%$ and also a high melting point of T_m = 144 °C was concluded from the DSC traces of nascent powders obtained from precipitation of the aqueous particle dispersions (Figure S3). Thus, the present synthetic method leads to a virtually perfect chain and crystallization is not disturbed by branching.

Chart 1. Chemical Structure of the New Water-Soluble κ^2-(N,O)-Salicylaldiminato Nickel(II) Methyl TPPTS Precatalyst

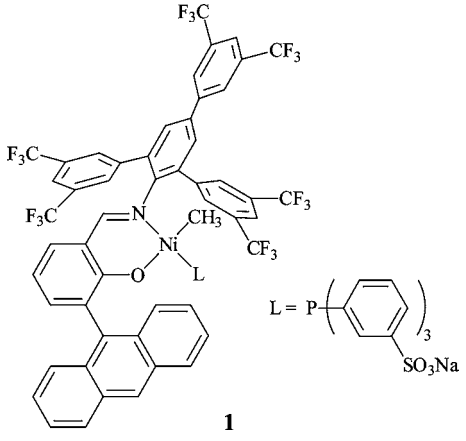

1

Concerning the origin of this unusually high order, one must consider the crystal formation process. The polymer is formed at a polymerization temperature of 10 °C. Both crystal growth and crystal formation rates, that is, the rate at which stems add to an existing growth front, and rates of nucleation of crystals are difficult to estimate: this temperature regime has not been accessible for studies of such a process, as traditional experimental approaches employ rapid quenching from the melt which is difficult to perform practically to such low temperatures as 10 °C. Observed initial rates of polymerization with **1** point to a chain growth rate on the order of 10 repeat units per second. Extrapolation of nucleation rate data[6] and crystallization rate data[7] suggests that crystallization occurs faster than this chain growth. This would correspond to incorporation of the chain as it grows by catalytic insertion steps directly into the crystal (Figure 2), and thus minimize the possibility to form larger chain segments with conformations unfavorable for the generation of crystalline order, like entanglements.

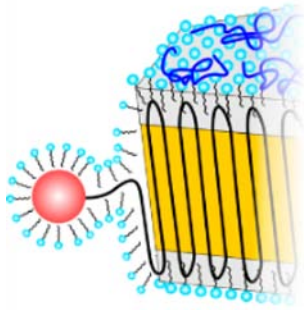

Figure 2. Polymer chain incorporation during formation of ideal PE-nanocrystals by catalytic insertion polymerization with a water-soluble Ni(II) catalyst.

Cryogenic transmission electron microscopy (cryo-TEM) of the dispersions shows well-defined nanocrystals with relatively narrow size distribution and a faceted shape (Figure 3). In particular, most of the crystals have a rectangular shape. This shape may be due to the fact that the crystals exhibit a monoclinic fraction as revealed by wide-angle X-ray scattering

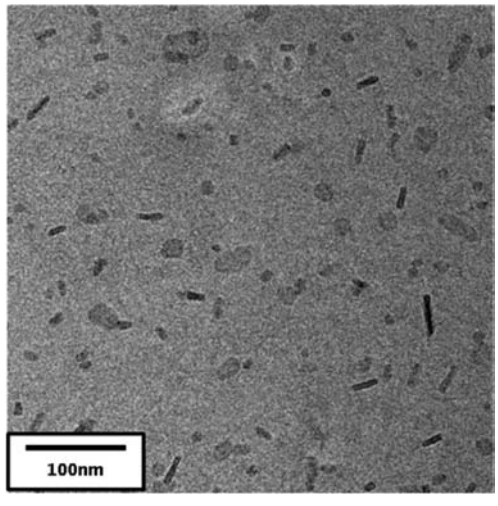

Figure 3. Cryo-TEM micrograph of the PE-nanocrystals in aqueous dispersion.

dx.doi.org/10.1021/ja4052334 | J. Am. Chem. Soc. 2013, 135, 11645−11650

(see the discussion of Figures S4 and S5 in the SI). Note that the amorphous layers are not visualized by cryo-TEM due to the small electron density contrast of the amorphous polymer layers compared with the vitrified water.

The micrograph shows a slightly bimodal size distribution which is corroborated by analysis by analytical ultracentrifugation (Figure S6). Attempted electron diffraction on single PE-nanocrystals failed to provide further information on the crystal structure, due to a rapid degradation of the crystals under the electron beam at room temperature.

Small-angle X-ray scattering (SAXS) was used for the comprehensive analysis of the PE-nanoparticle. SAXS also complements TEM in that it captures the entire ensemble of particles in the sample under study.

The platelet model used for the evaluation of these scattering data (Figure S7) consists of a crystalline lamella which is enclosed by two amorphous layers (Figure 4). Two additional

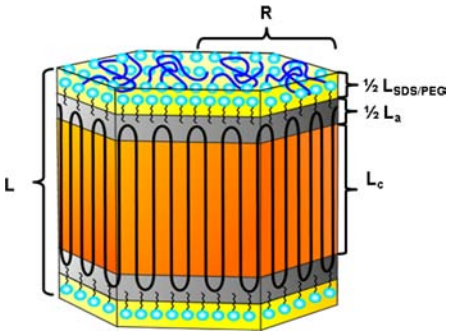

Figure 4. Scheme of the platelet-like structure of the nanoparticles.

layers on top and below describe adsorbed polyethylene glycol (PEG) together with the surfactant SDS that stabilizes the particles. Note that the addition of polyethylene glycol and ethylene glycol was necessary to avoid the formation of clathrates from water and ethylene at typical polymerization conditions (10 °C and 40 atm of ethylene). In general, the SAXS intensity can be described by

$$I(q, \phi) = \frac{N}{V} I_0(q) S(q) = \phi V_P (\Delta b)^2 P(q) S(q) \quad (1)$$

where q is the magnitude of the scattering vector ($q = (4\pi/\lambda)\sin(\theta/2)$, λ: wavelength, θ: scattering angle), N/V is the number density of the dispersed particles, and $I_0(q)$ is the scattering intensity deriving from single particle scattering. The particle volume fraction is expressed by ϕ, whereas V_P is the particle volume. The contrast is denoted by Δb. It describes the difference between the local scattering length densities to the surrounding medium. The form factor $P(q)$ describes the shape and the size of the particles whereas $S(q)$ is the structure factor describing the particle interactions. The scattering intensity of such a particle $I_0(q)$ can be calculated according to

$$I_0(q) = \int_0^1 F^2(q, x)\, dx \quad (2)$$

with

$$F(q) = 2\pi R \frac{J_1(qR\sqrt{1-x^2})}{q\sqrt{1-x^2}} \left(\Delta b_{SDS/PEG} \frac{\sin\left(\frac{qxL}{2}\right)}{\left(\frac{qx}{2}\right)} + \Delta b_a \frac{\sin\left(\frac{qx(L_a+L_c)}{2}\right)}{\left(\frac{qx}{2}\right)} + \Delta b_c \frac{\sin\left(\frac{qxL_c}{2}\right)}{\left(\frac{qx}{2}\right)} \right) \quad (3)$$

Here R is the radius of a circular platelet consisting of a crystalline layer of the height L_c sandwiched between layers of amorphous PE and adsorbed SDS as well as PEG as is shown in Figure 4. The faceted nanocrystals can be treated in good approximation as circular platelets for the SAXS analysis.[3,4] The heights of the amorphous PE regions are given by $L_a/2$, while L denotes the total height of the platelet. The electron contrasts are defined as $\Delta b_{SDS} = b_{SDS} - b_s$, $\Delta b_a = b_a - b_{SDS}$, and $\Delta b_c = b_c - b_a$, where b_a, b_c, b_s, and b_{SDS} are the electron densities of the amorphous PE layers, the crystalline PE layer, the solvent, and the SDS/PEG layers, respectively. Here the hydrocarbon tails of the SDS molecules contribute to the amorphous PE layers. The value of the electron density of the solvent b_s is determined by the concentrations of water and added glucose acting as contrast agent. Moreover, $J_1(x)$ denotes the cylindrical Bessel function of first order.

The overall PE-nanoparticle dimensions following from the fit of the scattering intensities are the average height of the crystalline layer $L_c = 8.8 \pm 1$ nm, the average total height of the amorphous layer $L_a = 2.1 \pm 0.5$ nm, and the height of the SDS and PEG layers $L_{SDS/PEG} = 1.0$ nm (Figure 4). The results of the contrast variation show that the PE-nanocrystals obtained with catalyst precursor **1** are characterized by a crystalline fraction of 82%. This significantly exceeds the degree of order found previously for nanocrystals of PE with remaining chain branches (χ(SAXS) = 70%).[4] The height $L_a/2 \approx 1$ nm of each of the two amorphous PE-layers is reasonably close to the theoretical minimum height of about 0.5 nm of tight loops found in recent computer simulation studies of adsorbed PE chains.[8,9]

The high crystallinity of the particles found by X-ray diffraction supports the assumption (vide supra) that crystallization occurs faster than the chain growth. The chain produced by a catalyst will be attached immediately to the growing crystal and no amorphous intermediate state intervenes. The consequences of this mechanism are immediately evident: The amorphous layer will be very small and will just assume the minimum size to accommodate a tight folding of the PE-chains. To this end, thermal annealing is also instructive. Annealing is not expected to increase the thickness of the amorphous layer considerably if no branches are present and no entanglements were formed during polymerization. The chains may diffuse through the crystal and the amorphous layers on top and below the lamella act as the wheels in a pulley by just changing the direction of the chains by 180°. We term this state 'ideal polyethylene nanocrystal' since the polymer chains are arranged in an ordered fashion without defects or entanglements. If, on the other hand, crystallization after polymerization proceeds through an intermediate state with little order, entanglements will be formed immediately which in turn will lead to a much thicker amorphous phase.

SAXS-investigations on annealed dispersions were conducted using samples in neat water having a slightly higher concentration vs the aforementioned studies (ω_{PE} = 2.6 wt

dx.doi.org/10.1021/ja4052334 | J. Am. Chem. Soc. 2013, 135, 11645−11650

%; see SI). Higher concentrations were used in order to obtain a good signal-to-noise ratio even at low contrast. For annealing, the dispersion of the nanocrystals was kept at a given temperature for 10 min. Typically, dispersions were stable under these conditions (T = 100−130 °C). During annealing at 150 °C, which is significantly above the melting temperature (Figure S3), small amounts of precipitate of the polymer were formed which were filtered off. Analysis was performed after cooling down to room temperature.

The SAXS intensities of the original sample together with the measured scattering intensities after annealing at 100, 115, 125, 130, and 150 °C are shown in Figure 5a (from bottom to top).

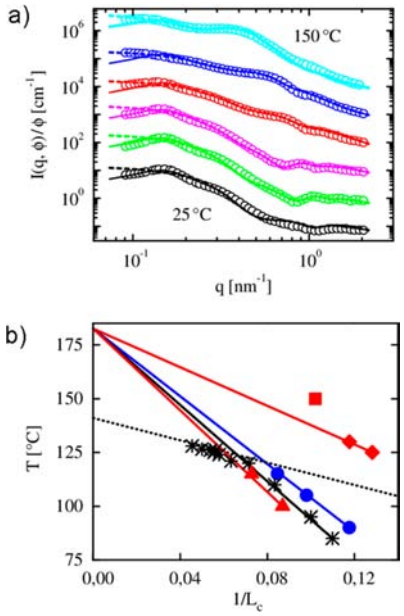

Figure 5. SAXS measurements of the polyethylene nanoparticles dispersed in pure water. (a) Measured scattering intensity $I(q, \phi)$ of polyethylene nanoparticles at 25 °C and after annealing at 100, 115, 125, 130 and 150 °C. For clarity, the five uppermost scattering intensities are shifted up by a factor of 10, 10^2,10^3, 10^4, and 10^5. The dashed lines represent the results of the modeling of the SAXS data for a dispersion of noninteracting particles and the solid lines of interacting particles, respectively. (b) Annealing temperatures (triangles: 100 °C, 115 °C, diamonds: 125 °C, 130 °C, square: 150 °C) as a function of the inverse height of the crystalline layer L_c together with the data obtained using PE with significant chain branches (circles).[4] The stars represent experimentally determined initial crystalline lamellar thicknesses of PE crystallized from the melt,[12] while the dotted line denotes the melting line.[13]

The lines in Figure 5a show the calculated results for noninteracting particles (dashed lines) and for interacting particles (solid lines) using the model parameters according to eq 3 as listed in Table 1.

Moreover, the radius R of the particles is chosen such that the number of PE-repeating units is independent of the annealing temperature as expected on physical grounds. For small magnitudes of the scattering vector q the calculated scattering intensities for noninteracting particles (dashed lines) and for interacting particles (solid lines) deviate due to strong repulsive electrostatic interaction between the particles due to the adsorbed SDS molecules (see the discussion in refs 3 and 4, and the SI).

Table 1. Structural Parameters of Annealed PE-Nanocrystals.[a]

T [°C]	L_c[nm]	L_a[nm]	b_c[nm^{-3}]
25	8.8	2.1	340
100	11.5	2.1	340
115	13.7	2.1	340
125	7.8	3.2	346
130	8.5	4.4	346
150	9.8	16.0	340

[a]Main parameters derived from the model fits to the scattering intensities shown in Figure 5a. The heights of the crystalline and amorphous PE layers are denoted as L_c and L_a, respectively, while b_c is the electron density of the crystalline PE layer. The standard deviation of the Gaussian size distribution is 1 nm for L_c and 0.5 nm for L_a, whereas b_c is considered a constant. The electron densities of the amorphous PE-layers b_a = 302 nm^{-3} and the SDS layers b_{SDS} = 397 nm^{-3} are independent of the annealing temperature.

The height L_c of the crystalline lamellae obtained by annealing at a given temperature demonstrates that annealing at 100 and 115 °C increases L_c markedly while the height L_a of the amorphous region remains constant (Table 1). Thus, crystallinity is increasing and after annealing at 115 °C the crystalline fraction is 88%. This finding supports the notion of an 'ideal PE-nanocrystal': The absence of branches allows the chains to diffuse through the crystal. The amorphous layers act as the wheels of a pulley as shown schematically in Figure 6; no entanglements within these layers impede the motion of the chains.

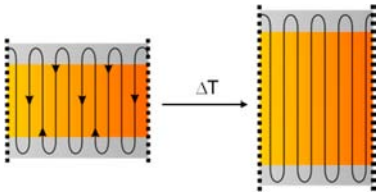

Figure 6. Mechanism of thermal annealing in an ideal PE-nanocrystal: The amorphous layers covering both platelets act as the wheels of a pulley just changing the direction of the chains. A moderate raise of the temperature induces sufficient mobility that allows the chains to move within the crystal. Hence, the thickness L_c of the crystalline phase is increased while the thickness L_a of the amorphous layers remains constant.

The surface free energy of the crystal is proportional to the slope of the annealing temperature T as a function of $1/L_c$ (Figure 5b) as suggested by the Gibbs−Thomson equation (see ref 10 and references therein) $T = T^{\infty}(1 - \alpha/L_c)$ with $\alpha = 2\sigma/\Delta h$, where Δh is the heat of fusion, σ the surface free energy of the lamellae, and T^{∞} the temperature limit referring to fully crystalline samples. In the limit of a large lateral size of the PE-nanocrystals ($R \gg L$), σ is the solvent−amorphous layer interfacial tension, while finite crystal size effects have been discussed in ref 11. The surface free energy of the 'ideal PE-nanocrystal' under consideration here is higher in comparison to the literature known crystals with branches.[4] Both molecular stiffness and the free energy needed to stabilize an amorphous loop increase with increasing branching ratio due to restriction of rotation and bending of the backbone chains by the side chains. Hence, crystals from perfect PE-chains should exhibit a higher surface energy as is found here.

dx.doi.org/10.1021/ja4052334 | J. Am. Chem. Soc. 2013, 135, 11645−11650

For comparison the stars represent experimentally determined initial crystalline lamellar thicknesses of PE crystallized from the melt,[12] while the dotted line denotes the melting line $T = 141.1\ °C - 259.7\ nm/L_c$ according to ref 13. Evidently, the temperatures $T^{\infty} = 182\ °C$ obtained by extrapolation of the three data sets below the melting line agree within experimental accuracy. This is to be expected since the influence of the amorphous regions on the crystallization (stars) and recrystallization (triangles, circles) processes is vanishing in the limit of infinitely long polymer chains.

The decrease of the crystalline height of PE-nanocrystals upon increasing the annealing temperature from 115 to 125 °C is rather unexpected. In the case of bulk PE this increase of temperature leads to further increase of L_c. For the nanocrystals under consideration here, this is not observed, but L_c decreases markedly while L_a is increasing. Further annealing leads to an increase of L_c again as expected from previous experiments.[4] However, the slope of the annealing temperature as a function of the inverse height of the crystalline layer is smaller ($\alpha = 2.46$ nm, upper red line in Figure 5b) as compared to the one in the lower annealing temperature regime ($\alpha = 5.20$ nm, lower red line in Figure 5b). Moreover, the increase of the amorphous part of the crystals is not only evident from L_a measured by SAXS but also from WAXS-measurements performed simultaneously with the SAXS measurements (see the discussion of Figure S5 in the SI). The small monoclinic fraction vanishes after annealing at 100 °C and the amorphous halo underneath the remaining reflections related to the orthorhombic modification is increasing. Thus, a crossing of the melting line (dashed line in Figure 5b) leads to a drastic change of the overall structure of the PE-nanocrystals. The increased mobility of the PE-chains at these temperatures has apparently affected the order in the crystals. Under these conditions, the shape of the nanocrystals seems to be mainly determined by the surface tension as discussed previously.[4] Hence, the dependence of L_c on T does not present a general phenomenon anymore but depends on the stabilizing agents used herein.

SUMMARY AND CONCLUSIONS

The novel water-soluble salicylaldiminato Ni(II)-methyl complex **1** produces highly ordered high molecular weight polyethylene nanocrystals devoid of branches at a low polymerization temperature of 10 °C in an aqueous medium. The particles formed are single 'perfect' ordered nanocrystals consisting of a single crystalline lamella covered by very thin amorphous layers, as revealed by combination of cryo-TEM and SAXS analysis. The unusually high degree of order found independently by SAXS and DSC results from crystallization during polymerization in the compartmented space of nanoparticles. An ordered deposition of the growing polymer chain on the nanocrystal growth front occurs as the chain is formed by the catalyst. This leaves no opportunity for entanglements to form, and an ideal nanoscale polymer crystal is formed under these conditions. This highly ordered structure is further corroborated by annealing studies, which show that below the melting point the chains can slip through the crystal in a well-behaved undisturbed fashion without increasing the size of the very thin amorphous layer.

The generic synthetic approach to highly ordered nanoscale polymer crystals by chain growth polymerization in nanoscopic confinement appears of future interest to address, among others, problems associated with entanglements in the processing of ultra high molecular weight polymers.

EXPERIMENTAL SECTION

Cryogenic Transmission Electron Microscopy. Studies were carried out using a Zeiss EM922 Omega transmission electron microscope (TEM) equipped with a cryo sample stage. Thin films of a diluted PE-nanocrystal dispersion supported on a copper grid were vitrified in liquid ethane at −183 °C.[14]

Small Angle X-ray Scattering. Experiments were carried out at the ID02 beamline at the European Synchrotron Radiation Facility (ESRF) in Grenoble (France). Scattering intensities were measured with the FReLoN 2D CCD detector at 1 and 2 m detector position. This setup covers a q-range of $0.05 < q < 2.9\ nm^{-1}$ and $0.09 < q < 4.9\ nm^{-1}$, respectively. A photon energy of 12.46 keV was selected, corresponding to a wavelength of $\lambda = 1$ Å. The samples were measured in a tempered 2 mm polycarbonate capillary at 25 °C. The obtained 2D scattering patterns were normalized to an absolute intensity scale and azimuthally averaged following the standard procedure to obtain the one-dimensional scattering profiles which were further averaged among the ten measurements. The sample was automatically pushed through the capillary to prevent radiation damage. The obtained scattering intensities were averaged during the data reduction process.

Wide Angle X-ray Diffraction. This was measured with a Bruker AXS D8 Advance diffractometer using the Cu-α line at $\lambda = 1.5406$ Å. The samples were measured as precipitated polymer powder in the range $10° < 2\theta < 80°$. Additionally, wide angle diffraction was measured during the SAXS experiments at ID02 beamline by operating the AVIEX PCCD-detector simultaneously. This option covers a q-range between $5 < q < 30\ nm^{-1}$.

Sample Preparation. The samples were prepared from a dialyzed stock dispersion of the polyethylene nanoparticles with a polymer weight fraction of 2.6 wt %. As additives the dispersion contained 0.13 wt % SDS for stabilization and 0.37 wt % of PEG that could not be removed by dialysis. Under these conditions the dispersion was stable over month.

For the contrast variation series the samples were diluted with a SDS solution to keep the surfactant concentration constant. In the following the PE-nanocrystal samples and the corresponding scattering background solutions were prepared by the addition of glucose. Glucose was purchased from Sigma Aldrich and used as received.

Polyethylene nanocrystals were annealed in dispersion at 100, 115, 125, 130 and 150 °C in a sealed glass vial for 10 min. The respective polymer weight fraction of the annealed samples was $\omega_{PE} = 2.6$ wt %.

The density of the polyethylene nanoparticles including the adsorbed additives was determined by densiometric measurements in a concentration series. A density of $\rho = 1.0024 \pm 0.001\ g\ cm^{-3}$ was determined for the nanoparticles including the adsorbed surfactant and PEG.

ASSOCIATED CONTENT

Supporting Information

Detailed experimental procedures, characterization data, and data analysis. This material is available free of charge via the Internet at http://pubs.acs.org.

AUTHOR INFORMATION

Corresponding Author

*E-mail: stefan.mecking@uni-konstanz.de and matthias.ballauff@helmholtz-berlin.de.

Author Contributions

The manuscript was written through contributions of all authors. All authors have given approval to the final version of the manuscript.

Notes

The authors declare no competing financial interest.

■ ACKNOWLEDGMENTS

We thank ESRF for the provision of synchrotron beam time. A.O. and S.M. thank the Stiftung Baden-Württemberg for financial support. We thank Antje Völkel and Helmut Cölfen for analytical ultracentrifugation analysis.

■ ABBREVIATIONS

DSC, differential scanning calorimetry; SAXS, small-angle X-ray scattering; WAXS, wide-angle X-ray scattering; TEM, transmission electron microscopy

■ REFERENCES

(1) (a) Smith, P.; Lemstra, P. J. *J. Mater. Sci.* **1980**, *15*, 505. (b) Rastogi, S.; Lippits, D. R.; Peters, G. W. M.; Graf, R.; Yao, Y.; Spiess, H. W. *Nat. Mater.* **2005**, *4*, 635. (c) Rastogi, S.; Yao, Y.; Ronca, S.; Bos, J.; van der Eem, J. *Macromolecules* **2011**, *44*, 5558. (d) Matsui, S.; Fujita, T. *Catal. Today* **2001**, *66*, 63.

(2) (a) Bauers, F. M.; Thomann, R.; Mecking, S. *J. Am. Chem. Soc.* **2003**, *125*, 8838−8840. (b) Göttker-Schnetmann, I.; Korthals, B.; Mecking, S. *J. Am. Chem. Soc.* **2006**, *128*, 7708−7709.

(3) Weber, C. H. M.; Chiche, A.; Krausch, G.; Rosenfeldt, S.; Ballauff, M.; Harnau, L.; Göttker-Schnetmann, I.; Tong, Q.; Mecking, S. *Nano Lett.* **2007**, *7*, 2024−2029.

(4) Rochette, C. N.; Rosenfeldt, S.; Henzler, K.; Polzer, F.; Ballauff, M.; Tong, Q.; Mecking, S.; Drechsler, M.; Narayanan, T.; Harnau, L. *Macromolecules* **2011**, *44*, 4845−4851.

(5) Ballauff, M. *Adv. Eng. Mater.* **2011**, *13*, 793−802.

(6) (a) Loo, Y.-L.; Register, R. A.; Ryan, A. J. *Phys. Rev. Lett.* **2000**, *84*, 4120. (b) Kraack, H.; Deutsch, M.; Sirota, E. B. *Macromolecules* **2000**, *33*, 6174.

(7) (a) Waheed, N.; Rutledge, G. C. *J. Polym. Sci., Part B: Polym. Phys.* **2005**, *43*, 2468. (b) Ratajski, E.; Janeschitz-Kriegl, H. *Colloid Polym. Sci.* **1996**, *274*, 938. (c) Wagner, J.; Phillips, P. J. *Polymer* **2001**, *42*, 8999.

(8) Ramos, J.; Martinez-Salazar, J. *J. Polym. Sci., Part B: Polym. Phys.* **2011**, *49*, 421−430.

(9) Minoia, A.; Chen, L.; Beljonne, D.; Lazzaroni, R. *Polymer* **2012**, *53*, 5480−5490.

(10) Strobl, G. *Prog. Polym. Sci.* **2006**, *31*, 398−442.

(11) (a) Wang, Y.; Rafailovich, M.; Sokolov, J.; Gersappe, D.; Araki, T.; Zou, Y.; Kilcoyne, A. D. L.; Ade, H.; Marom, G.; Lustiger, A. *Phys. Rev. Lett.* **2006**, *96*, 028303. (b) Metatla, N.; Palato, S.; Commarieu, B.; Claverie, J. P.; Soldera, A. *Soft Matter* **2012**, *8*, 347.

(12) Barham, P. J.; Chivers, R. A.; Keller, A.; Martinez-Salazar, J.; Organ, S. J. *J. Mater. Sci.* **1985**, *20*, 1625−1630.

(13) Wunderlich, B.; Czornyj, G. *Macromolecules* **1977**, *10*, 906−913.

(14) Lunkenbein, T.; Kamperman, M.; Li, Z.; Bojer, C.; Drechsler, M.; Förster, S.; Wiesner, U.; Muller, A. H. E.; Breu, J. *J. Am. Chem. Soc.* **2012**, *134*, 12685−12692.